Higher-order spectral modelling of the diffraction force around a vertical circular cylinder

H. Bredmose and S. J. Andersen

DTU Wind Energy, Denmark, hbre@dtu.dk

1 INTRODUCTION

The present paper is a continuation of the paper by the same authors at the workshop of 2016 (Bredmose & Andersen, 2016). While the 2016 paper outlined the concept for the proposed higher-order spectral force model, the present paper details the validation of its linear and nonlinear implementation.

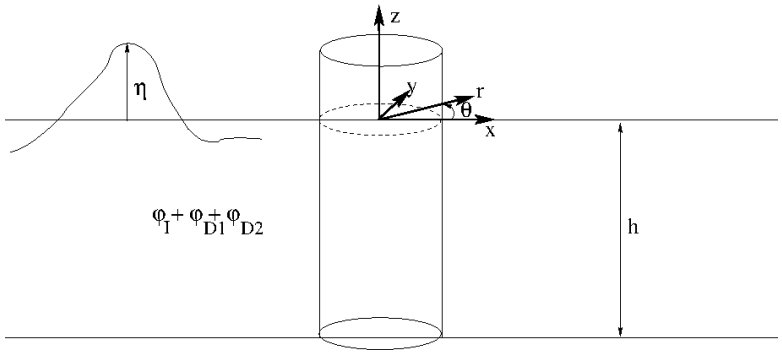

Figure 1: Definition sketch for diffraction calculation around vertical circular cylinder.

2 MODEL CONCEPT

The purpose of the higher-order spectral force model is to bridge the gap between 1) the MacCamy & Fuchs (1954) diffraction theory that is only linearly valid and 2) the combination of fully nonlinear wave kinematics with the Morison or Rainey (1995) force models which is restricted to slender structures. The goal is thus a force model that incorporates full diffraction and (almost) full nonlinearity. Taking inspiration from Ducrozet et al. (2014), the model is further formulated for the diffracted wave field only, assuming that the incident wave field is known. This allows application of pre-computed incident wave fields from fully nonlinear models, for example the OceanWave3D solver (Engsig-Karup et al., 2009), with possible application to offshore wind turbine monopile foundations (Bredmose et al., 2016; Schløer et al., 2016). A definition sketch is show in figure 1. We denote the depth h and the cylinder radius r_0.

The central element of the model is the decomposition of the free surface and velocity potential (η, ϕ) into an incident field (I), a linear diffraction field (D1) and the nonlinear diffracted field (D2)

$$\begin{pmatrix}\eta\\ \phi\end{pmatrix} = \begin{pmatrix}\eta\\ \phi\end{pmatrix}_I + \begin{pmatrix}\eta\\ \phi\end{pmatrix}_{D1} + \begin{pmatrix}\eta\\ \phi\end{pmatrix}_{D2}. \tag{1}$$

Cylindrical (r, θ, z) coordinates are adopted, where $\theta = 0$ is the main wave direction and the z-axis points upwards from the still water level at the cylinder centre. The fields are further expanded in

cylindrical Bessel functions

$$\eta_{ID1} = \sum_{p=0}^{P}\sum_{j=1}^{N}\left[A_{pj}J_p(k_{pj}r) - \mathrm{Re}\left\{\left(A_{pj} + \frac{\mathrm{i}\omega_{pj}}{g}B_{pj}\right)\frac{J'_{pj}}{H'_{pj}}H_p^{(1)}(k_{pj}r)\right\}\right]\cos(p\theta) \tag{2}$$

$$\phi_{ID1} = \sum_{p=0}^{P}\sum_{j=1}^{N}\left[B_{pj}J_p(k_{pj}r) - \mathrm{Re}\left\{\left(B_{pj} + \frac{\mathrm{i}g}{\omega_{pj}}A_{pj}\right)\frac{J'_{pj}}{H'_{pj}}H_p^{(1)}(k_{pj}r)\right\}\right]\cos(p\theta)\frac{\cosh(k_{pj}(z+h))}{\cosh(k_{pj}h)} \tag{3}$$

where $k_{pj}/r_{\max}$ is the j'th root of the first kind Bessel function of order p; $H_p^{(1)}$ is the first kind order p Hankel function; $J'_{pj} \equiv \partial_r J_p(k_{pj}r)|_{r=r_0}$ and $H'_{pj} \equiv \partial_r H_p^1(k_{pj}r)|_{r=r_0}$. The J-terms represent the incident wave field (I) and the Hankel functions, which are outward propagating waves represent the (D1) field, similar to the MacCamy & Fuchs (1954) solution for monochromatic linear waves. The coefficients of the Hankel functions are chosen such that $\eta_r = \phi_r = 0$ at $r = r_0$. Upon transformation of the incident wave field to the Fourier-Bessel space, the above expansion thus allows construction of the (D1) field.

The (D2) field is the remaining unknown field and is solved through the fully nonlinear free surface conditions

$$\eta_t = \left[1 + \epsilon^2\left(\nabla\eta\right)^2\right]\tilde{\phi}_z - \epsilon\nabla\tilde{\phi}\cdot\nabla\eta \quad , z = \eta \tag{4}$$

$$\phi_t = -g\eta - \tfrac{1}{2}\epsilon\left[\left(\nabla\tilde{\phi}\right)^2 + \tilde{\phi}_z^2\left(1 - \epsilon^2\left(\nabla\eta\right)^2\right)\right] \quad , \quad z = \eta, \tag{5}$$

where $\tilde{\phi}$ denotes evaluation at the free surface. We note that both the incident field (I) and the total field (ID1D2) is a solution to these equations, at the incident free surface η_I and total free surface η_{ID1D2} respectively. We may therefore isolate the time derivatives of the (D2) field by

$$\begin{pmatrix}\eta\\ \phi\end{pmatrix}_{D2,t} = \mathcal{RHS}\left\{\begin{pmatrix}\eta\\ \phi\end{pmatrix}_{ID1D2}\right\} - \mathcal{RHS}\left\{\begin{pmatrix}\eta\\ \phi\end{pmatrix}_{I}\right\}, \tag{6}$$

where $\mathcal{RHS}$ is a short-hand notation for the right hand side of (4)–(5). The full nonlinearity of the free surface conditions are handled through the Higher-Order Spectral method (HOS), where the velocity potential is Taylor expanded from the still water level and ordered with respect to powers of the wave steepness ϵ

$$\epsilon\tilde{\phi} = \sum_{m=1}^{M}\sum_{n=0}^{m-1}\epsilon^m\frac{\eta^n}{n!}\left(\frac{\partial}{\partial z}\right)^n\phi_0^{m-n}. \tag{7}$$

The expansion gives rise to a recursive method where the vertical velocity at the free surface can be computed by successive approximation of the velocity potential at still water level, ϕ_0, see e.g. West et al. (1987); Dommermuth & Yue (1987). The vertical velocity at the free surface can next be computed by re-application of this expansion, after operation of the ∂_z operator on the ϕ_0 field. This can be done in the spectral domain through the known z-variation of (2)–(3).

Now, with knowledge of the incident wave field (I), addition of the diffracted (D1) field and knowledge of the instantaneous (D2) field, (6) enables time-integration for the nonlinear diffraction field $(\eta, \phi)_{D2}$. Once solved, the force on the cylinder is obtained by direct pressure integration

$$F = -\rho\int_{\theta=0}^{2\pi}\int_{z=-h}^{\eta}\left[-\phi_t - \tfrac{1}{2}\left(\phi_r^2 + (\phi_\theta/r)^2 + \phi_z^2\right)\right]\cos\theta\,\mathrm{d}z\,r_0\mathrm{d}\theta \qquad , \qquad r = r_0 \tag{8}$$

where $(\phi_t, \phi_r, \phi_\theta, \phi_z)$ at the cylinder wall are computed from the spectral expansion (2)–(3).

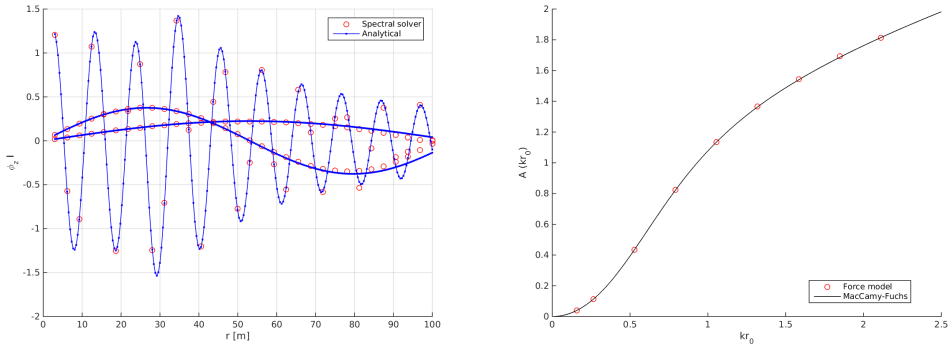

Figure 2: Left: Check of spectral ∂_z operator for various wave lengths. Right: Check of MacCamy-Fuchs force coefficient for linear wave forcing.

3 VALIDATION OF THE LINEAR SOLVER

The linear solver is first validated by a check of the spectral ∂_z operator associated with (2)–(3). A domain of radius $r \in [3; 100]$ m and depth $h = 25$ m is considered. The r-direction is resolved with 32 points and 24 Bessel functions at each order p. For the θ direction, we utilize the symmetry around the inline wave direction and resolve $\theta \in [0; \pi]$ also with 32 points. Figure 2(left) shows $\phi_{0I,z}$, i.e. the vertical derivative of the incident wave potential at $z = 0$ for the three wave numbers $k = 2\pi\ (0.5, 1, 10)/r_{\text{max}}$, obtained by the spectral solver. The results are shown at $\theta = 7\pi/64$ and compared to the known analytical expansion of MacCamy & Fuchs (1954). The circles show the spectral results for the actual points of calculation, while the analytical solution is shown as a finer resolved curve. A good match is seen, with the largest deviations occuring towards the outer boundary.

Another test is provided by computation of the linear force through (8). Here, the incident wave field is given to the solver, which next adds the diffracted wave field and computes the force by integration up to $z = 0$. The analytical solution is known from MacCamy-Fuchs theory to be

$$F = \frac{2\rho g H}{k^2} A(kr_0) \tanh(kh) \cos(\omega t - \delta(kr_0)) \tag{9}$$

where $A(kr_0) = [J_1'(kr_0)^2 + Y_1'(kr_0)^2]^{-1/2}$, Y_1 is the first order Bessel function of second kind and $\delta(kr_0)$ is a phase shift. Figure 2(b) shows the value of $A(kr_0)$ as obtained by the spectral method, compared to the analytical solution. A perfect match is seen for the various values of kr_0.

4 VALIDATION OF THE NONLINEAR SOLVER

The nonlinear part of the model has been validated by computation of the vertical velocity at the free surface w_I for an incident wave, also in the cylindrical domain. The free surface elevation and free surface potential for a fully nonlinear stream function wave (Fenton, 1988) was given as input to the HOS scheme, implemented to third order in the cylindrical coordinates. The result for w_I is compared to the target solution of the stream function theory in figure 3(left) for $\theta = \pi/64$. Wave steepnesses of $kH/2 = (1, 2, 4, 6, 8, 10)\pi/100$ were applied. A general good match is seen, with some visible numerical oscillations for the largest steepnesses. The right panel depicts a relative error measure for w_I, compared to slopes of 1st, 2nd and 3rd order accuracy. Beyond a threshold of about 0.002, the relative error is seen to be of third order. The absolute error is thus of fourth order in wave steepness, agreeing with the third-order implementation of the HOS scheme.

5 NEXT STEPS

After validation of the linear solver and the HOS implementation in the cylindrical domain, current work focuses on the calculation of the nonlinear D2 field through (6) and the resulting force time

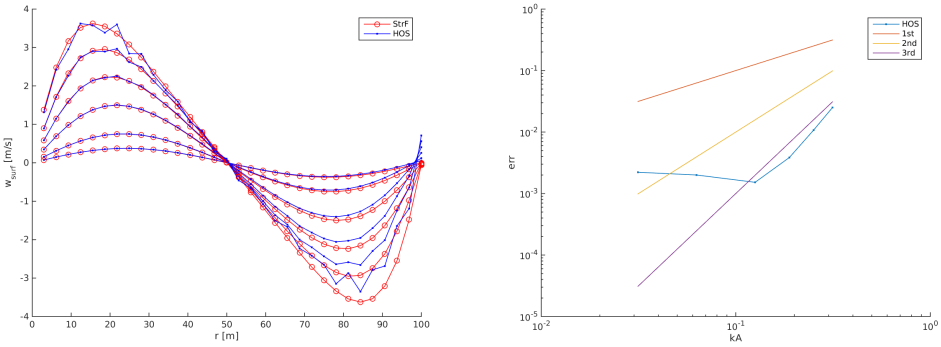

Figure 3: Left: Vertical velocity at free surface by cylindrical third-order HOS scheme, compared to stream function wave solution for varying kA. Right: Convergence of solution for vertical velocity for varying wave steepness kA.

series. A challenge here is the short wave length of the diffracted waves relative to the incident wave length scale. Results from this will be presented at the workshop. Besides providing an accurate force model for steep waves, the solver is expected to provide insight into the nature of the higher-order force components of first regular and next irregular waves for monopile-type structures.

The work was partly carried out in the DIMSELO project, which is a Knowledge-building Project for Industry funded by the Norwegian Research Council (NRC) under the ENERGIX program. The project is also funded by its industry partners Statoil and Statkraft. The projects research partners are IFE, NTNU and DTU.

References

Bredmose, H. & Andersen, S. J. (2016), Towards a higher-order spectral force model for vertical circular cylinders, *in* '31st Int. Worshop on Water Waves and Floating Bodies', Plymouth, Michigan, US.

Bredmose, H., Dixen, M., Ghadirian, A. & authors), . (2016), 'DeRisk — Accurate prediction of ULS wave loads. Outlook and first results', *Energy Procedia* **94**, 379–387.

Dommermuth, D. G. & Yue, D. K. P. (1987), 'A high-order spectral method for the study of nonlinear gravity waves', *J. Fluid Mech.* **184**, 267–288.

Ducrozet, G., Engsig-Karup, A. P. & Bingham, H. B. (2014), 'A nonlinear wave decomposition model for efficient wave-structure interaction. Part A: Formulation, validation and analysis', *J. Comp. Physics* **257**, 863–883.

Engsig-Karup, A., Bingham, H. B. & Lindberg, O. (2009), 'An efficient flexible-order model for 3D nonlinear water waves', *J. Comp. Phys.* **228**, 2100–2118.

Fenton, J. D. (1988), 'The numerical solution of steady water wave problems', *Computers & Geosciences* **14**(3), 357–368.

MacCamy, R. C. & Fuchs, R. A. (1954), Wave forces on piles: A diffraction theory, Technical Report 69, US Army Corps of Engineers. Beach Erosion Board.

Rainey, R. C. T. (1995), 'Slender-body expressions for the wave load on offshore structures', *Proc. Roy. Soc. London Series A. Math. and Phys. Sci.* **450**(1939), 391–416.

Schløer, S., Bredmose, H. & Bingham, H. B. (2016), 'The influence of fully nonlinear wave forces on aero-hydro-elastic calculations of monopile wind turbines.', *Marine Structures* **50**, 162–188.

West, B. J., Brueckner, K. A., Janada, R. S., Milder, D. M. & Milton, R. L. (1987), 'A new numerical method for surface hydrodynamics', *J. Geophys. Res.* **92**(C11), 11803–11824.